Robotics and Computer-Integrated Manufacturing 28 (2012) 425–436

Contents lists available at SciVerse ScienceDirect

Robotics and Computer-Integrated Manufacturing

journal homepage: www.elsevier.com/locate/rcim

Navigation of automated guided vehicles using magnet spot guidance method

Sok-Yong Lee [a,*], Hai-Won Yang [b]

[a] Department of Technical Center for Advanced Manufacturing, Sam Hyun Co., Ltd., South Korea
[b] Department of Electronic, Electrical, Control & Instrumentation Engineering, Hanyang University, Seoul, South Korea

ARTICLE INFO

Article history:
Received 26 July 2010
Received in revised form
7 October 2011
Accepted 14 November 2011
Available online 26 January 2012

Keywords:
AGV
Magnet spot guidance
Fuzzy control
Hall-effect sensor

ABSTRACT

Automated guided vehicle systems (AGVSs) are used to transport goods and products in most manufacturing systems. In this research, we use a cylindrical magnet spot, which is widely used in industrial AGVSs, to develop a guidance system for indoor AGV navigation. This paper describes the navigation and control system of an AGV by magnet spot guidance with a differential drive. Furthermore, Hall-effect sensors, encoders, and counters are employed to achieve control and continuous guidance. Existing guidance methods use a gyro sensor and dead reckoning with encoders to calibrate against steering angle errors. Here, the maximum value of the magnetic flux density of the magnet spot, which is obtained by the Hall-effect sensor, is used to calibrate against steering angle errors and as a navigation guide for the AGV. Furthermore, real-time corrections for wheel-skidding errors are accomplished with a fuzzy controller. Thus, high-precision continuous guidance with stable and satisfactory navigation at high speeds is achieved. This guidance method was applied to real manufacturing processes in a ceramic plant and steel-bar reinforcement plant to examine its control ability, stability, and effectiveness. The proposed method was found to be robust to disturbances and uncertainty problems during tracking.

1. Introduction

In recent years, automated guided vehicle systems (AGVSs) have been employed in many applications such as factory automation, warehouses, container terminals, golf carts, and hospitals. In particular, the application of AGVSs to factory automation in flexible manufacturing systems (FMSs) has become popular because manufacturing costs and the number of defects in manufactured goods are reduced, while productivity, flexibility, and stability improve [1]. In AGV guidance systems, various methods are employed to obtain effective control, such as inductive wire guidance [2–4], laser guidance [5,9], and visual servoing using cameras [10]. The inductive wire guidance method provides the greatest system stability factor and is the most popular one.

In the inductive wire guidance method, the path of most AGVs is determined by an inductive wire embedded under the floor; navigation is autonomously accomplished along the wire by the detection of a magnetic flux generated by the inductive wire or by tracking a tape pasted on the floor path.

A technique known as dead reckoning is used to measure the displacement of each wheel; here, an encoder is installed in the driving parts and the changes in the position or displacement at each section are computed to calculate the current position from the initial position. However, this method is not appropriate for long-distance navigation owing to the continuous accumulation of measurement errors. Some guidance methods use a separate device such as a gyro sensor to calibrate against steering angle errors.

In this study, a magnet spot is installed on the floor surface of an AGV navigation system, and a Hall-effect sensor is used for the measurement of the magnetic flux density from the magnet spots. The maximum value of the magnetic flux density is used for the navigation guide. The steering errors during navigation are calibrated with a fuzzy controller. All the input and output variables were quantified for real-time control; moreover, a look-up table was constructed from the output values obtained from fuzzy reasoning to save the time for the fuzzy inference.

This paper is organised as follows. Section 2 describes the methods employed by existing AGV guidance systems and the related problems, while Section 3 explains the proposed navigation system that employs magnet spot guidance. Section 4 discusses the experimental environment. Finally, Section 5 experiment and performance analysis examines the stability and effectiveness of the proposed controller during the real-time navigation of an AGV in a manufacturing facility. Section 6 concludes the paper.

* Corresponding author. Tel.: +82 43 878 4041; fax: +82 43 878 8105.
E-mail address: lm8619@unitel.co.kr (S.-Y. Lee).

0736-5845/$ - see front matter © 2011 Elsevier Ltd. All rights reserved.
doi:10.1016/j.rcim.2011.11.005

2. Conventional AGVS guidance methods and related problems

2.1. Inductive wire guidance

The inductive wire AGV guidance method is based on the basic principle of generation of a magnetic field around a conductor as a result of current flowing through it. This magnetic field is stronger around the conductor and weaker away from the conductor. An electromotive force proportional to the strength of the magnetic field is generated at the end terminal of the coil when current passes through it. When an AGV is positioned at the centre of an inductive wire that is placed under the ground, maximum voltage is induced, while minimum or no voltage is induced at the left and right coils symmetric to the reference point (centre) of the inductive wire.

This method has the advantage of enabling navigation through accurate position tracking; moreover, precise position control is possible. However, its implementation cost is extremely high because the floor surface has to be cut for navigation guidance and wire has to be embedded in the floor. Moreover, periodic maintenance is required and it is difficult to make modifications to the process layout [2–4].

2.2. Laser guidance navigation

Laser guidance navigation involves the use of laser beams for the AGV navigation; laser beam reflections from a reference point are detected by a scanner, which measures the distance and angle to each target location. The output coordinates are marked on a control board, and the location of the AGV is computed for its navigation.

In this method, the floor surface does not have to be cut, and moreover, it is not restricted by the floor condition; further, free navigation of the AGV in the visual field between the sensor and reference patterns is possible. However, the method is limited by increases in the system cost; moreover, the precision of position control is influenced by the nature of the surrounding environment, such as height, distance to the reflector, presence of interfering obstacles, and narrow navigation areas. For instance, as the distance to the reflector increases, the position precision error increases [9].

2.3. Visual servoing guidance navigation with camera monitoring

The visual servoing guidance navigation method with camera monitoring identifies the position of a landmark relative to AGV, and it requires accurate camera corrections for the target localisation. If this requirement is not met, there can be problems of localisation errors due to incorrect mapping from an image space to workspace. In addition, if the error in the mapping of a landmark image is serious, there can be a problem of unwarranted movements of the AGV in the workspace [10].

3. Proposed magnet spot guidance navigation method

3.1. Structure and kinematic model of AGV

The driving method proposed in this paper is a differential drive method that consists of two independent driving wheels at the geometrically central part and two unpowered bi-directional wheels for the forward and backward directions.

The differential driving method employs a steering method to use the speed difference between the left and right wheels, and its mechanical parts are simple in that the same motor operates both steering and driving. In addition, it allows turning centred on the two driving wheels during the spin-turn rotation drive of the AGV. The differential drive-type AGV also allows for changes in the y-axis and θ-axis positions in two-dimensional space. Note that three coordinates are required for position reference. The coordinates x and y denote the midpoint of two driving wheels, while the angle θ is the angle between the navigation axle and driving direction.

In Fig. 3-1, the coordinates (x, y) represent the midpoint of an AGV in a fixed coordinate frame $\{X, Y\}$, while θ denotes the steering angle of a moving AGV coordinate frame against the axes of a fixed coordinate frame. o_c is the midpoint of the driving axle and is at a position enabling initial measurements [11]. In general, for the design of the control input, the kinematic modelling of the wheel-driving AGV system assumes that the midpoint of the driving axle is at the centre of mass of the AGV for the design of control input.

In an absolute coordinate X–Y frame, the AGV position is determined by the coordinates (x_c, y_c) of the centre of mass of AGV o_c and θ_c, the angle between the longitudinal axis and X-axis.

Assuming that wheels roll and do not skid between the floor surface and wheel due to the effect of inertia and gravity, the angular velocity w_c and linear velocity v_c at o_c are expressed as follows, respectively:

$$w_c(t) = \frac{w_L(t) - w_R(t)}{D} r = \frac{v_L(t) - v_R(t)}{D} \tag{3.1}$$

$$v_c(t) = \frac{w_L(t) + w_R(t)}{D} r = \frac{v_L(t) + v_R(t)}{D} \tag{3.2}$$

Here w_L, w_R, and v_L, v_R denote the angular and linear velocities, respectively, of the left and right driving wheels, respectively; D, the distance between the wheels of the differential-drive AGV; r, the wheel radius.

In addition, the kinematic model for the x- and y-axes components of v_c and θ_c, can be expressed by the following

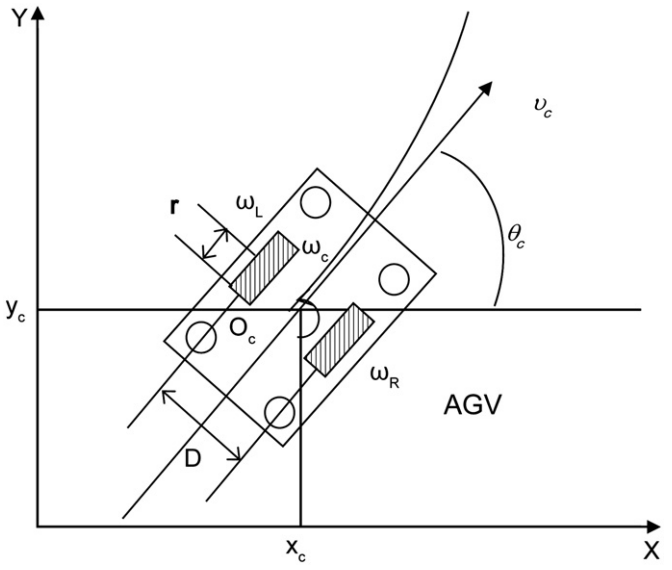

Fig. 3-1. AGV model with two independent driving wheels. θ_c, body of steering angle; o_c, centre of mass; D, distance between left and right wheels; r, radius of wheel; w_L, angular velocity of the left driving wheel; w_R, angular velocity of the right driving wheel; v_R, linear velocity of the left driving wheel; v_R, linear velocity of the right driving wheel; v_c, linear velocity of centre of mass; w_c, angular velocity of centre of mass.

equation:

$$\dot{x}_c(t) = v_c(t)\cos\theta_c(t)$$
$$\dot{y}_c(t) = v_c(t)\ \sin\theta_c(t)$$
$$\dot{\theta}_c(t) = w_c(t) \tag{3.3}$$

Eq. (3.4) expresses the kinematical position state as a state matrix of the centre of mass, which is influenced by the linear velocity and control input of the angular velocity:

$$u(t) = [v_c(t),\ w_c(t)]^T$$
$$\begin{bmatrix} \dot{x}_c(t) \\ \dot{y}_c(t) \\ \dot{\theta}_c(t) \end{bmatrix} = \begin{bmatrix} \cos\theta_c(t) & 0 \\ \sin\theta_c(t) & 0 \\ 0 & 1 \end{bmatrix} \begin{bmatrix} v_c(t) \\ w_c(t) \end{bmatrix} \tag{3.4}$$

In addition, Eq. (3.5) can be derived from Eqs. (3.1) and (3.2), and the navigation of AGV can be determined by the control input of v_L, v_R:

$$u(t) = \begin{bmatrix} v_c(t) \\ w_c(t) \end{bmatrix} = \begin{bmatrix} \frac{1}{2} & \frac{1}{2} \\ \frac{1}{D} & -\frac{1}{D} \end{bmatrix} \begin{bmatrix} v_L(t) \\ v_R(t) \end{bmatrix} \tag{3.5}$$

When Eqs. (3.1) and (3.2) are substituted into Eqs. (3.3) and (3.4), and both sides are integrated, the positional movements of the AGV and its posture information, $x_c(t)$, $y_c(t)$, and $\theta_c(t)$ can be obtained as follows:

$$x_c(t) = x_0 + \frac{r}{2}\int_0^t [w_L(t) + w_R(t)]\cos\theta_c(t)dt \tag{3.6}$$

$$y_c(t) = y_0 + \frac{r}{2}\int_0^t [w_L(t) + w_R(t)]\sin\theta_c(t)dt \tag{3.7}$$

$$\theta_c(t) = \theta_0 + \frac{r}{D}\int_0^t [w_R(t) - w_L(t)]dt \tag{3.8}$$

In other words, if the initial posture is known from the above equation and the angular velocity of two driving wheels is obtained from the encoder, the position and steering angle of AGV can be obtained. Note that the linear and angular velocities of the two driving wheels of the AGV are controlled by the rotation speed.

The ultimate goal of path tracking is to find a method to track the AGV in the desired trajectory by computing its linear velocity $v_c(t)$, and the angular velocities of the two driving wheels, $w_c(t)$, after knowing the coordinates. The actual navigation should also consider such unpredictable factors such as the inertia of AGV, skidding between the floor and wheel, wear of the driving wheel, sensor error, tension in the belt between motor and driving parts (axle), and reducer gear backlash.

3.2. Control system of the proposed AGV

The AGV employed in this study consists of a magnet spot, Hall-effect sensor, guidance controller, driving axle and driver, guide recognition and position recognition device, wireless communication system, hydraulic system, and laser safety device. Its dimensions are width of 1660, length of 2850, and height of 508, and it can carry a maximum of 10 t. Further, it is controlled by a programmable logic controller (PC–PLC) system, which is shown in Fig. 3-2. The AGV is operated using the differential driving method, and there are two independent driving wheels for using the speed difference between the left and right wheels for steering. The same motor is used for navigation and position rotation. In other words, there are totally six wheels—two driving wheels and four idle wheels (casters).

As shown in Fig. 3-2, driving wheels are present on the left and right of the body centre, and a brushless DC (BLDC) motor is used to run them. An encoder and a sensor, and they can be used to calculate the position and steering angle of the AGV.

External errors in path tracking result from wheel skidding or floor curvature; external sensors are required to measure them since these errors cannot be measured by internal sensors such as encoders.

In previous studies, a gyro sensor has been used as the external sensor to correct the steering angle error along with the encoder. However, in this study, an encoder and a counter were installed in the driving wheel to correct for the steering angle error, and the

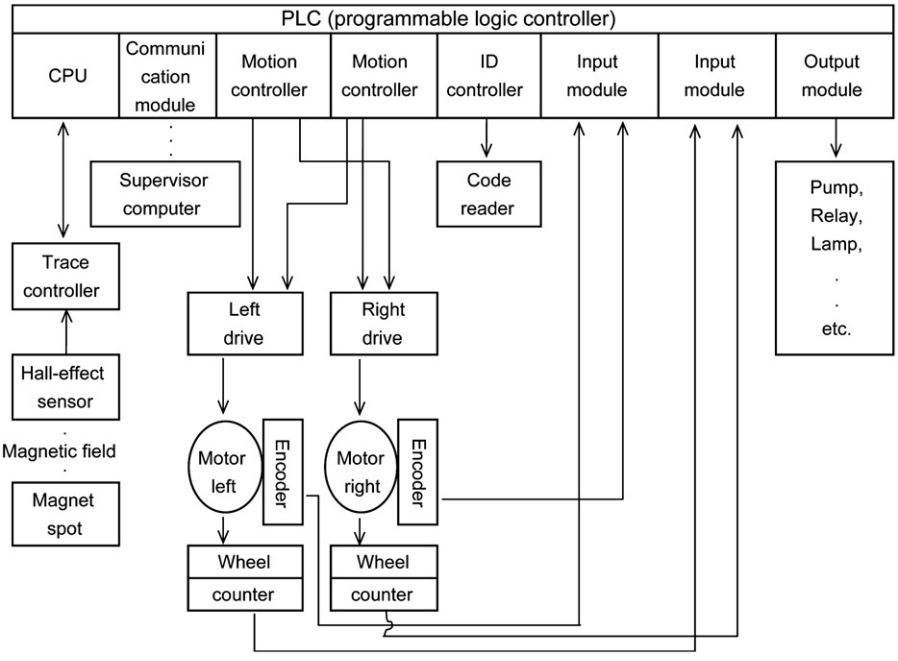

Fig. 3-2. Structure and schematic of PC-PLC-based AGV system.

magnetic flux density (Gauss) distribution of the magnet spot was measured using a Hall-effect sensor. This measurement was then used as guidance for AGV, and the skidding error of the wheel was adjusted on a real-time basis.

3.3. Magnetic dipole model of magnet spot

For AGV navigation, the magnetic flux density of the magnet spot is obtained from the relationship between the magnet spot and Hall-effect sensor on the basis of the central axis of the magnetic flux density distribution. A mathematical model for the magnetic flux density is required to predict the position of the magnet spot and to identify the central axis of the distribution of the maximum magnetic flux density.

In this study, the magnet spot is assumed to be a magnetic dipole to predict position a mathematical model. Under this assumption, the components (B_x, B_y, and B_z) of the three-axle magnetic flux density can be derived from the magnet spot in three-dimensional space. This makes is possible to predict the position and central axis of the maximum magnetic flux density distribution using a Hall-effect sensor away from the magnet spot; it also becomes possible to control the steering angle using the central axis of the magnetic flux density distribution.

The magnetic dipole potential for the magnet spot can be expressed as given in Eq. (3.9); in this manner, it becomes possible to compute the magnetic flux density of the magnet spot in three-axle space from the position of the Hall-effect sensor away from the magnet spot [5]:

$$U = \frac{M\cos\theta}{4\pi\mu_0 r^2} = \frac{Mz}{4\pi\mu_0}(x^2+y^2+z^2)^{3/2}[A] \tag{3.9}$$

where U is the potential of magnetic dipole, M is the Moment of magnetic dipole, and μ_0 is the permeability of free space $4\pi \times 10^{-7}$ H/m:

$$r = \sqrt{(x^2+y^2+x^2)}$$

The magnitudes of the three-axial components of the magnetic flux density (B_x, B_y, and B_z) can be expressed as Eqs. (3.10)–(3.12), respectively, from the relationship between the magnetic dipole potential and magnetic field [5]:

$$B_x = \frac{3}{4}k\frac{xz}{(x^2+y^2+z^2)^{5/2}} \text{ [Gauss]} \tag{3.10}$$

$$B_y = \frac{3}{4}k\frac{yz}{(x^2+y^2+z^2)^{5/2}} \text{ [Gauss]} \tag{3.11}$$

$$B_z = \frac{1}{4}k\frac{2z^2-x^2-y^2}{(x^2+y^2+z^2)^{5/2}} \text{ [Gauss]} \tag{3.12}$$

here $k : Ma/4\pi$, a : unit coefficient, B_x and B_y denote magnetic flux density as measured by Hall-effect sensor at the front or rear side and left and right sides, respectively, of the magnet spot, while B_z is the magnetic flux density obtained from the height of the magnet spot and Hall-effect sensor (Fig. 3-3).

As shown in Figs. 3-4 and 3-5, the distribution of the magnetic flux density of the magnet spot in three-axle (x, y, z) directions is continuously measured when the Hall-effect sensor, which is installed in the AGV, passes through the magnet spot. The measured distribution of the magnetic flux density is used for the analysis of the relationship between the magnet spot and Hall-effect sensor to locate the current position of the AGV; in this manner, the steering angle of the AGV can be controlled for effective navigation of the AGV from its current position.

To reiterate, the x axis is the forward or backward driving direction; y axis, the left and right directions from the central line of the AGV; z axis, the upper or lower directions between the central line of the AGV and installed sensor. In this study, the magnetic flux density at a fixed height is measured. The Hall-effect sensor installed in the AGV continuously measures the distribution of the magnetic flux density from the central axis of the magnet spot, i.e., the central path of AGV.

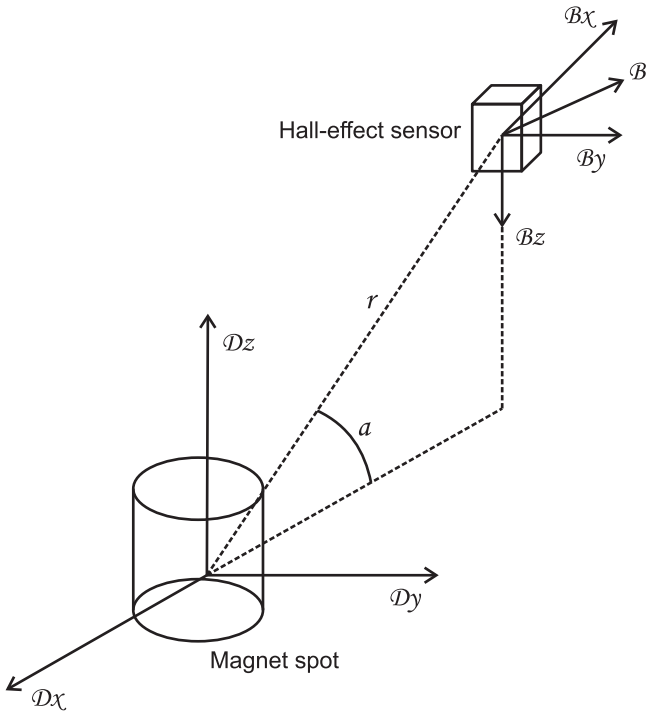

Fig. 3-3. Magnetic dipole model.

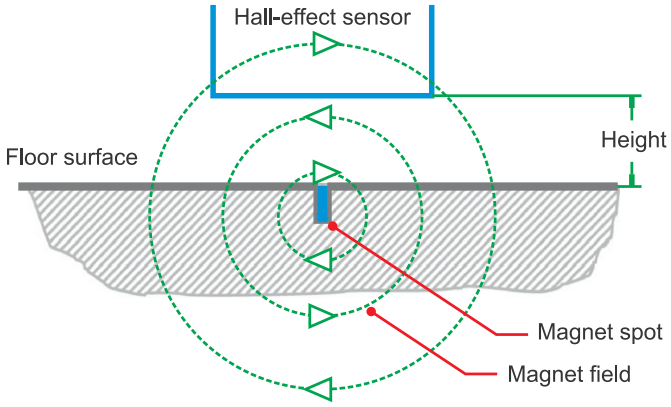

Fig. 3-4. Principle of generation of magnetic spot and magnetic field.

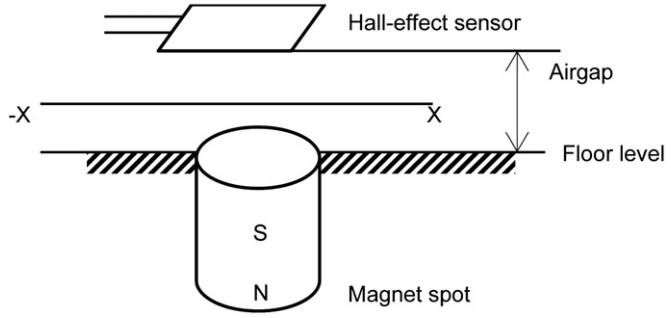

Fig. 3-5. Installation of Hall-effect sensor in relation to magnet spot.

Using the measured distribution of the magnetic flux density, the lateral distance and angle of any AGV deviation on either side of the central axis of the magnet spot are computed in real time, and the driving error is corrected; thus, the desired navigation of the AGV is accomplished.

3.4. Magnet spot and hall-effect sensor

The magnet spot is cylindrical and is installed on the floor surface. There is no definite rule to determine the distance between one magnet spot and the next one, for it depends on the navigation node type and precision. The Hall-effect sensor for the detection of the magnet spot is based on the PC-PLC, and it is used to detect the distribution of magnetic flux density; the detection has high precision for small magnet spots (N-pole or S-pole) on the floor. When the next magnet spot appears, the AGV system produces new position data coordinates (x, y, θ) from the feedback of the Hall-effect sensor. In other words, the Hall-effect sensor is used to identify the movement and position of the AGV, and it updates the AGV position as it passes the magnet spot.

Fig. 3-5 illustrates the installation of the Hall-effect sensor with respect to the magnet spot, while Fig. 3-6 depicts the relationship among magnetic flux density, magnetic flux density distribution, and air gap at the instant the Hall-effect sensor passes the magnet spot [6].

3.5. AGV navigation by magnet spot guidance

The magnet spot guidance navigation of an AGV uses the Hall-effect sensor to detect a small magnet installed on the floor and measure the distribution of the magnetic flux density for computing the moving distances of the wheel and the steering angle. This system is a continuous inductive wire guidance navigation system. The Hall-effect sensor calculates the distance moved from the magnet spot as the AGV deviates from its track and provides information for new data updates for navigation. Small magnet spots are discontinuously and randomly installed on the floor surface of the virtual navigation path for guiding the AGV navigation.

The magnet spots for AGV guidance are installed irregularly on the navigation floor, and this inductive wire guidance represents an AGV guidance method that has been revised for dealing with the difficulties in repairing wire installations. In addition, compared with the laser guidance method, the method is not restricted by the surrounding environmental conditions and has the advantage of simpler control, lower price, high precision, and better space utilisation since spin-turning is allowed. The steering control and navigation control are independently controlled by two BLDC motors.

For AGV guidance, the components of the Hall-effect sensor are installed at the forward, backward, and central locations of the AGV. In this study, the AGV system assumes the centre of the magnet spot installed on the floor to be the guide path of the AGV. The magnetic flux density distribution as measured by the Hall-effect sensor with its embedded Hall-effect element will then have the maximum value at the centre of the Hall-effect sensor. Moreover, the magnetic flux density detected by the Hall-effect sensors on both sides is assumed to be symmetrical for the purpose of the navigation design. In such a case, the AGV maintained high precision and realized high-speed navigation. The magnet spot guidance system detects the displacement at both sides from the centre of the Hall-effect sensor and obtains the information for determining the correction value by calculating the lateral distance deviation from the guide path at the instant the AGV passes the next magnet spot. An encoder is used to measure the distance to the next magnet spot, and the encoder data is reset at the instant the AGV passes the magnet spot.

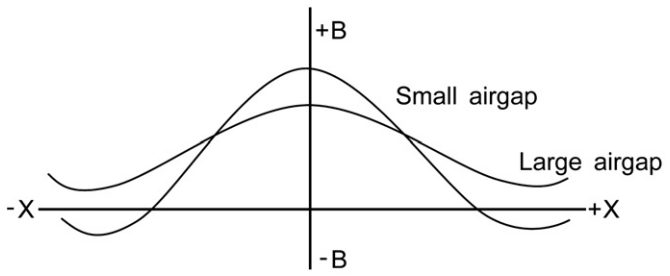

Fig. 3-6. Relationship among magnetic flux density, magnetic flux density distribution, and air gap at the instant Hall-effect sensor passes the magnet spot.

The position recognition system of the AGV measures the error by dead reckoning of the Hall-effect sensor when moving and corrects for this error. In this study, the method for computing the current steering angle is applied by revising the corrections for the cumulative measuring error due to dead reckoning using the central axis data of the magnetic flux density distribution.

3.6. Dead reckoning control method for AGV

In Fig. 3-1, the differential driving AGV has three sets of Hall-effect sensors—at the front, middle, and central parts. The front, rear, and central Hall-effect sensors are used to guide the forward, backward, and rotational movements of the AGV, respectively. The forward, backward, and rotational movement of the AGV is controlled by the speed of the left and right BLDCs as well as motor rotations. As shown in Fig. 4-3, when the left and right BLDC motor speeds are identical, it navigates forward or backward; otherwise, it rotates around the centre point.

In general, the algorithms for AGV navigation can be classified into the following two types: (a) algorithms to determine the location of AGV and its errors, and (b) algorithms to execute the control command to minimise the position error as quickly as possible.

The magnetic flux density information obtained from the magnet spot, encoder, and counter is used to calculate the lateral distance and steering angle errors of the AGV.

3.7. AGV position tracking based on dead reckoning algorithms for encoder and counter sensor

The position tracking of an AGV is accomplished by dead reckoning based on the number of pulses from the encoder and counter; the encoder measures the rotations per minute (rpm) of the BLDC motor when an AGV moves and calculates the distance moved. The distances moved along a straight line and during rotation are measured. Since the dead reckoning method is a very inaccurate method (due to problems such as slipping of the wheel), it is generally used only in short-distance navigation.

The dead reckoning algorithm estimates the current position by adding increments to the previous position at each sampling zone on a real-time basis. When the sampling interval, Δt, increases along the moved distances, (Δx, Δy, $\Delta\theta$), and the speed at all sampling zones is assumed to be identical, the distance moved by an AGV, Δs, and the increment in the angle, $\Delta\theta$, can be expressed using $t=nT$ as follows [8]:

$$\Delta x = \Delta s \cos\left(\theta + \frac{\Delta\theta}{2}\right) \tag{3.13}$$

$$\Delta x = \Delta s \cos\left(\theta + \frac{\Delta\theta}{2}\right) \tag{3.14}$$

$$\Delta\theta = \frac{\Delta s_R - \Delta s_L}{D} \tag{3.15}$$

$$\Delta s = \frac{\Delta s_R + \Delta s_L}{2} \tag{3.16}$$

Here $(\Delta x, \Delta y, \Delta\theta)$=path travelled in the last sampling interval, Δs_R, Δs_L=travelled distances for the right and left wheels, respectively. D is the distance between the two wheels of a differential-drive AGV.

The current position is calculated using the speed of the wheel and change in its speed. The current position on the reference coordinates is computed by the AGV position at $t=nT$ (current sampling time), which is the sum of the position increment from the previous sampling step and the position at the previous sample step, $t=(n-1)T$.

$$x(k+1) = x(k) + \Delta s(k)\cos\left(\theta[k] + \frac{\Delta\theta[k]}{2}\right) \tag{3.17}$$

$$y(k+1) = y(k) + \Delta s(k)\sin\left(\theta[k] + \frac{\Delta\theta[k]}{2}\right) \tag{3.18}$$

$$\theta(k+1) = \theta(k) + \Delta\theta(k) = \theta(k) \tag{3.19}$$

3.8. Measurement of navigation distance (odometric reading)

The encoder and counter are installed on the driving wheel, and the increment angle at every sampling period $\Delta t_k = t_{k+1} - t_k$ is measured. The measurement of the navigation distance (odometric reading) is used to predict the linear velocity $\overline{v}(t_k)$ and the angular velocity $\overline{w}(t_k)$.

The increment error in the encoder is caused by the steering angle error. The linear and angular velocities obtained by this procedure are compared with the measured values that will be described in Section 5.1. When the error range is within a reference value (standard), each controller is fed back to operate the controller. When the reference voltage of the driving motor is applied to the BLDC motor, the motor navigates the AGV with the desired speed and path on a real-time basis.

The angular velocity displacement of the wheel, as measured by the encoder during the sampling time T_s, is denoted as Δs_r, Δs_l, r is the radius of the driving wheel of the AGV. When the RPM of the left and right wheels are identical, the number of pulses from the left and right encoders is also identical. The displacements of the linear velocity and angular velocity of AGV can then be expressed as $\Delta s = (r/2)(\Delta w_R + \Delta w_L)$ and $\Delta\theta = (r/2R)(\Delta w_R - \Delta w_L)$, respectively.

The estimation of the posture at time $t_k = kT_s$ can be expressed by the following equation:

$$\hat{q}_k = \begin{bmatrix} \hat{x}_k \\ \hat{y}_k \\ \hat{\theta}_k \end{bmatrix} = \hat{q}_{k-1} + \begin{bmatrix} \cos\overline{\theta}_k & 0 \\ \sin\overline{\theta}_k & 0 \\ 0 & 1 \end{bmatrix} \begin{bmatrix} \Delta s \\ \Delta\theta \end{bmatrix} + n \tag{3.20}$$

$$\overline{\theta}_k = \dot{\theta}_{k-1} + \frac{\Delta\theta}{2} \tag{3.21}$$

This position recognition of the AGV uses the driving estimation method; n is the random noise caused by such irregular variables as slipping motions of wheels, resolution of encoder, mechanical parameter errors, and radius variations in the wheel due to load changes and road conditions.

3.9. Design of fuzzy algorithm for correction of AGV navigation errors

A fuzzy algorithm is used to calculate the future output value for each input; it stores the data as a look-up table so that real-time control is possible. In this manner, the straight movements of the AGV can be navigated at a constant speed. When there is a change in the steering angle, the speed of the AGV is also changed to minimise deviations from the guide path. When the AGV is moving in a straight line but is moved to the left side due to uneven floors, wearing, or slipping of the wheel, etc., the AGV is made to move to the right side so that it returns to the guide path.

When the AGV is moving correctly on the guide path, the navigation speed is high. As a result, when the AGV deviates from the guide path, moving away from it, the navigation error is corrected at the high speed. In such a case, when the AGV approaches the navigation path, the speed is decreased to correct for the navigation error and to track the guide path again. Finally, when the AGV returns back to the guide path again, its speed is increased again.

In other words, the navigation algorithm is designed such that the AGV can track the guide path quickly and accurately. The two input variable parameters used as variable conditions in this study are the lateral distance error (d) away from the guide path and the steering angle error (θ_e) in the moving direction of the AGV.

An output variable must be selected for the navigation; this is the steering angle of the AGV. This study selected the following fuzzy set for the input variables and the output variable.

Let us examine three typical cases in order to establish basic rules:

(1) If the steering angle error θ_e and lateral distance error d are zero, then the steering angle θ is zero, and navigation speed v_s is "Fast Speed."
In other words, if $\theta_e = Z$ and $d = Z$.
Then $\theta = Z$ and $v_s = FS(LF \cdot RF)$.

(2) If θ_e is "Left Small" and d is "Left Near," θ is "Right Small" and v_s is "Right Slow Speed ."
In other words, if $\theta_e = LS$ and $d = LN$.
Then $\theta = RS$ and $v_s = RS$.

(3) If θ_e is "Right Large" and d is "Right Far," θ is "Left Big" and v_s is "Left Fast Speed."
If $\theta_e = RL$ and $d = RF$,
Then $\theta = LB$ and $v_s = LF$.

The following fuzzy set was established for the input variable parameters and the output variable parameter. Figs. 3-7 and 3-8 shows the membership function for the input variable parameters for tracking the guide path. Fig. 3-7 shows the angle between the AGV and guide path (θ); here, LL: Left Large; LS: Left Small; ZE: Zero Equal; RS: Right Small; RL: Right Large.

The fuzzy variable LL implies a large steering angle error on the left side of the reference guide path, while ZE implies that the

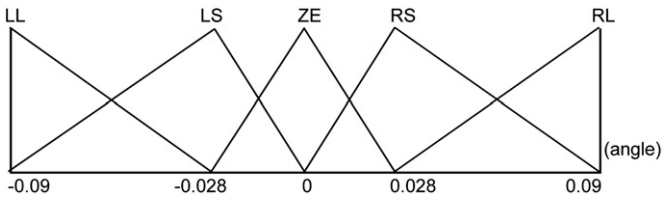

Fig. 3-7. Membership function of input variable parameter for steering angle error (θ_e) between AGV and guide path.

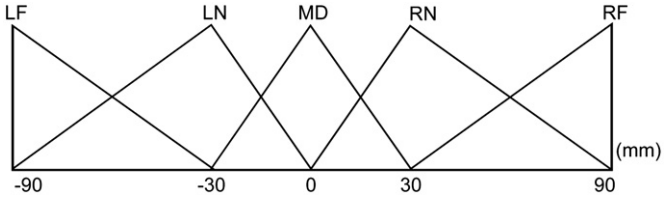

Fig. 3-8. Membership function of input variable parameter for lateral distance error (d) between AGV and guide path.

AGV is moving on the centre of the guide path and there is no steering angle error.

Fig. 3-8 shows the lateral distance error (d) between the AGV and guide path; the notations are as follows: LF: Left Far; LN: Left Near; MD: Middle; RN: Right Near; RF: Right Far. In other words, the fuzzy set can be expressed as follows. $d \in$ {LF (Left Far), LN (Left Near), MD (Middle), RN (Right Near), RF (Right Far)}. The fuzzy variable LF implies that the AGV deviates far right to the reference guide path; MD implies that the AGV is navigating right on the reference guide path; RN implies that the AGV is moving near the right side of the reference guide path.

The membership function for the output parameter for tracking the guide path was set as follows. Table 3-1 shows the fuzzy output rule for the steering angle (θ) of the AGV; the notations can be expanded as follows: LL (Left Large), LS (Left Small), ZE (Zero Equal), RS (Right Small), and RL (Right Large).

In other words, the fuzzy set can be expressed as follows. $\theta \in$ {LL (Left Large), LS (Left Small), ZE (Zero Equal), RS (Right Small), RL (Right Large)}.

The fuzzy variable LL implies that the AGV has to be significantly steered to the left; ZE implies straight navigation without steering angle manipulation; RS implies a slight steering of the AGV to the right.

Fig. 3-9 illustrates the fuzzy outputs for the angular velocity of the AGV, and the notations are described as follows: LB: Left Big; LS: Left Small; Z: Zero; RS: Right Small; RB: Right Big.

Fig. 3-10 shows the fuzzy output for the linear velocity of the AGV, and notations are described as follows: LF: Left Fast; LS: Left Slow; Z: Zero; RS: Right Slow; RF: Right Fast.

The angular velocity is determined by the differences in the angle between the centre of AGV and guide path and the AGV navigation angle. Depending on whether this value is positive or negative, the AGV rotates either to the left or to the right, respectively.

Table 3-1
Fuzzy rule for output parameters of AGV steering angle (θ) and distance (d).

Distance	Angle				
	LL	LS	ZE	RS	RL
LF	RL	RL	RL	RS	ZE
LN	RL	RS	RS	ZE	LS
MD	RL	RS	ZE	LS	LL
RN	RS	ZE	LS	LS	LL
RF	ZE	LS	LL	LL	LL

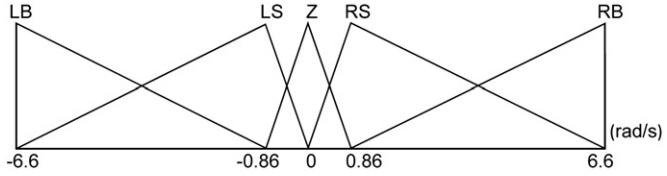

Fig. 3-9. Membership function of output variable parameters for angular velocity of the AGV.

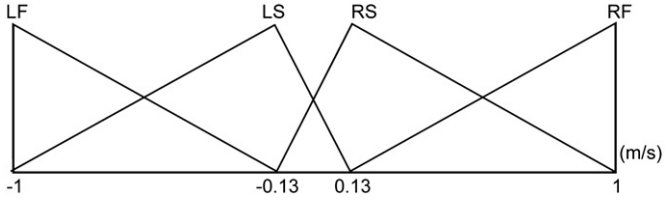

Fig. 3-10. Membership function of output variable parameter for linear velocity of the AGV.

The fuzzy control rule for the AGV tracking the guide path is set as shown in Tables 3-1, 3-2, and 3-3.

The guide path tracking by fuzzy control makes it convenient to set fuzzy rule. In addition, the fuzzy rule should be applied on a real-time basis for the AGV to navigate along the guide path safely, and the current state of the AGV should be recorded.

In this study, the membership function for the input parameters was a trigonometric membership function, and the estimation was conducted by Mamdani's MAX–MIN method.

Additionally, the defuzzifier method for the computation of the output from AGV navigation used he centre-of-gravity method. The AGV of this study is controlled by fuzzy rules with two input variables. This process should be employed with care because the number of rules, the number of input variable parameters for each rule, and the shape of the membership function determine the performance and property of the controller.

Here, the method of setting the fuzzy control rule followed expert experiences and fuzzy control rules, representing knowledge of control in linguistic expressions (Figs. 4-1 and 4-2).

Table 3-2
Fuzzy control rule for angular velocity (w).

Distance	Angle				
	LL	LS	ZE	RS	RL
LF	RB	RL	RL	RS	Z
LN	RB	RS	RS	Z	LS
MD	RB	RS	Z	LS	LB
RN	RS	Z	LS	LS	LB
RF	Z	LS	LB	LB	LB

Table 3-3
Fuzzy control rule for linear velocity (v).

Distance	Angle				
	LL	LS	ZE	RS	RL
LF	RF	RS	RS	RS	LF
LN	RF	RS	RS	RS	LF
MD	RF	RS	LF RF	LS	LF
RN	RS	RS	LS	LS	LF
RF	RS	LS	LS	LS	LF

Fig. 4-1. Magnet spot used in the experiment.

Fig. 4-2. Real-time navigation of AGV applied to actual manufacturing process (ceramic plant and steel-bar reinforcement plant).

4. Experimental environment

4.1. Structure and major parameters of AGV system

The dimensions of the AGV are 1660 mm (width) × 2850 mm (length) × 508 mm (height), and independently operating left and right wheels are fixed at the centre for forward and backward driving. Two casters are installed in the forward direction and two are installed in the backward direction. The major parameters of the AGV are described below:

AGV Mass (weight): 2100 kg.
Maximum transport weight: 10,000 kg.
Maximum speed: 80 m/min.
Ordinary operating speed: 60 m/min.
Voltage and capacity: 96(V) DC, 240(AH).
Distance between left and right wheels (D): 1255 mm.
Radius of wheel (r): 150 mm.
Distance between centre of mass and initial (first) Hall-effect sensor: 1080 mm.

4.2. Navigation patterns of AGV system

Fig. 4-3 illustrates the navigation patterns of the differential-drive AGV [7]. If the left and right BLDC motors operate at identical speeds, the AGV drives straight forward or straight backward. Otherwise, when one of the BLDC motors operates faster than the other one, the AGV will curve or follow an arc. If one of the motors operates in the opposite direction and at the same speed as the other motor, the AGV will rotate around the centre point of the AGV.

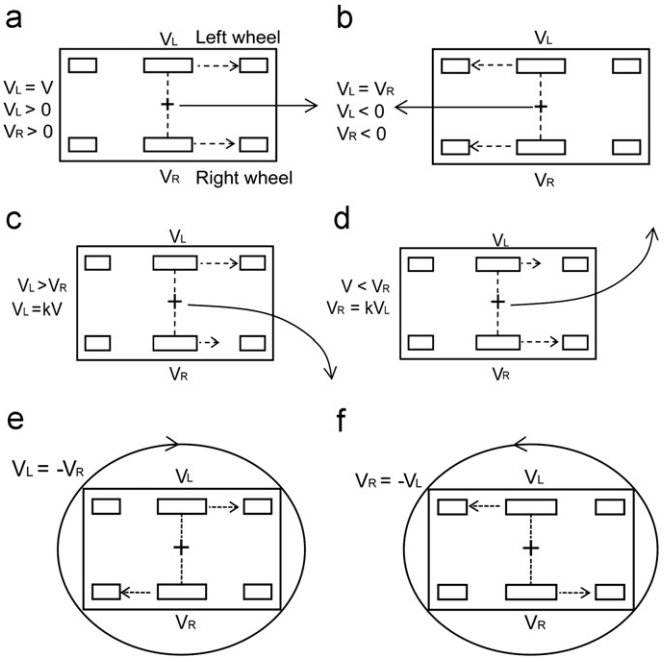

Fig. 4-3. Navigation and rotation patterns of differential-drive AGV. (a) Driving straight, forward; ($v_L = v_R$, $v_L > 0$, $v_R > 0$); (b) driving straight, backward ($v_L = v_R$, $v_L < 0$, $v_R < 0$); (c) turning right curve ($v_L > v_R$, $v_L = kv_R$); (d) turning left curve ($v_L < v_R$, $v_R = kv_L$); (e) counter-clockwise turning on the centre spot ($v_R = -v_L$, $v_R > 0$); (f) clockwise turning on the centre spot ($v_L = -v_R$, $v_L > 0$).

4.3. Real-time navigation of differential-drive AGV

The AGV is navigated using a host computer (supervisor computer); from Eq. (4.1), $w_R = w_L$, $v_R = v_L$, the radius of rotation (R) becomes infinite, $R = \infty$. This implies that the AGV is being navigated straight forward ($v_L = v_R$, $v_L > 0$, $v_R > 0$) and straight-backward ($v_L = v_R$, $v_L < 0$, $v_R < 0$).

If the differential-drive AGV deviates from the navigation guide path, it swerves to the left ($v_L < v_R$, $v_R = kv_L$) or right ($v_L > v_R$, $v_L = kv_R$). This situation is regarded as a navigation error and requires retracking of the guide path. In such a situation, there is a need for error corrections so that the maximum magnetic flux density from the magnet spot moves to the centre of the guide path.

The distance between nodes is measured by an encoder installed on the central axis of the AGV wheel, and this distance data is compared with the data computed by the Hall-effect sensor and controller to calculate the steering angle of the AGV. When the AGV deviates from the guide path, the Hall-effect sensor continually checks for the magnet spot installed on the floor surface. If this verification data differs from the encoder data by a value greater than a reference value, the AGV should immediately halt.

4.4. Real-time rotation of differential-drive AGV

The radius of rotation of the AGV wheel, R, has the following relationship with angular velocity (w_L, w_R) and linear velocity

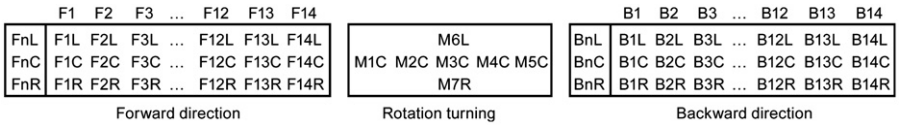

Fig. 4-4. Layout of Hall-effect sensor for magnet spot detection.

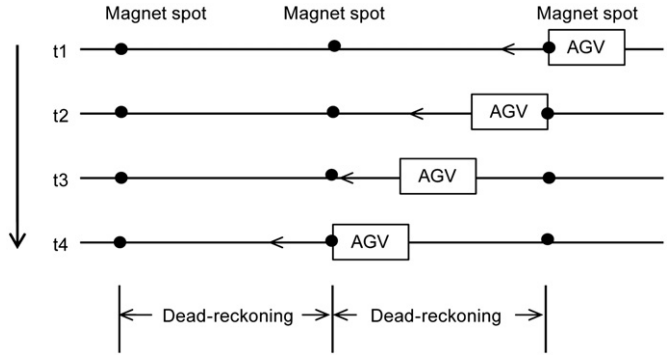

Fig. 4-5. Normal navigation state and dead reckoning navigation state.

$(v_L,\ v_R)$ when it is not slipping; $v_R = rw_R$, $v_L = rw_L$. Here, r is the wheel radius.

Thus, the radius of rotation of the wheel can be expressed as follows:

$$R = \frac{D}{2}\frac{(w_R + w_L)}{(w_R - w_L)} = \frac{D}{2}\frac{(v_R + v_L)}{(v_R - v_L)} \tag{4.1}$$

If $R=0$, when $w_R = -w_L$, $v_R = -v_L$, the AGV will rotate in its place around the centre.

Hence, if the differential-drive AGV has R equal to 0, it has the advantage of being able to navigate in a narrow environment; this implies that it can result in maximum efficiency in minimum space.

The AGV is navigated real-time with clockwise $(v_L = -v_R,\ v_L > 0)$ and counter-clockwise rotations $(v_R = -v_L,\ v_R > 0)$. This represents the case when the distribution of the magnetic flux density of the Hall-effect sensor, M_{3C}, has the maximum value while the distribution of the magnetic flux density of $M_{6L} = M_{7R}$ has the minimum value.

4.5. Layout of hall-effect sensor

Hall-effect sensors are installed in three rows of 14 steps, and seven Hall-effect sensors are located at the centre of AGV for rotation-turning, as shown in Figs. 4-1 and 4-4.

5. Experiment and performance analysis

Experiments were performed with three AGV systems (Fig. 4-5) and a 900-node transport system in an actual transportation environment in order to examine the effectiveness of the proposed method of this study, as illustrated in Figs. 4-2 and 5-1. In addition, the position at the straight navigation path and AGV turning were manoeuvred by the dead reckoning method.

5.1. Guidance method when hall-effect sensor passes a magnet spot upon straight navigation

Fig. 5-2 illustrates the distribution of the magnetic flux density (Gauss) when the linear velocity, initial angular velocity, lateral distance error, and steering angle error are $v = 1\,m/s$, $w = 0\,\text{rad/sec}$, $d = 0$, $\theta_e = 0$, respectively, i.e., when the Hall-effect sensor passes magnet spots upon straight navigation. The sampling time Δt is set at 0.1 s.

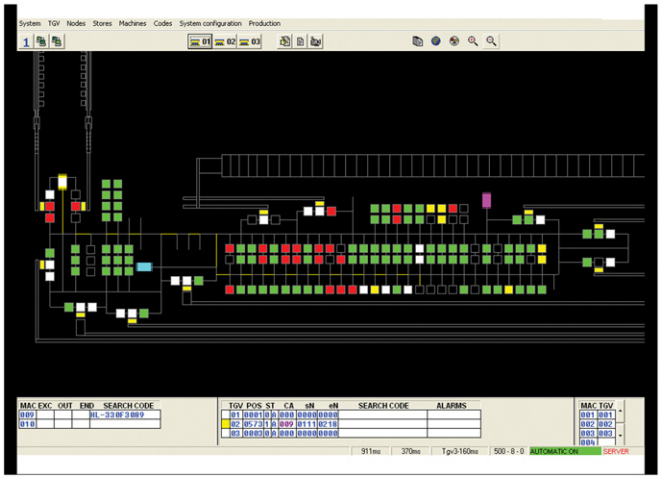

Fig. 5-1. Production line for actual experiment.

Fig. 5-2 shows the distribution of the magnetic flux density (Gauss) measured by the Hall-effect sensor passing through magnetic spots during straight forward navigation. The magnet spots are fixed on the floor surface, and Hall-effect sensors navigate while scanning the magnet spots and collecting data.

In the above figure, $F_1 \sim F_{14}$ represent rows of Hall-effect sensors.
F_{nL} means Hall-effect sensors at F_{1L}–F_{14L} (left of 1st row–left of 14th row).
F_{nC} denotes F_{1C}–F_{14C} (centre of 1st row–centre of 14th row).
F_{nR} indicates F_{1R}–F_{14R} (right of 1st row–right of 14th row).
$(t) \sim (t+13)$ represent the scanning steps.

The guide path can be constructed by connecting the points of maximum magnetic flux density.

In other words, the F_{nC} line is used as the guide path for the AGV navigation, and this method make the discontinuous guide path have the same effect as a continuous guide path. Thus, F_{1C}–F_{14C} (centre of 1st row–centre of 14th row) represents the centre line of the AGV navigation path.

Fig. 5-3 shows the distribution of the magnetic flux density (Gauss) measured by the Hall-effect sensor passing through magnetic spots during straight forward navigation. In the case of straight AGV navigation, the condition where disturbance is generated in the steps $(t+3)$ and $(t+4)$ is shown, and the figure shows that in this case the reference path is followed for error correction.

5.2. Dead reckoning method when magnet spot is not detected by hall-effect sensor during straight navigation

From Fig. 5-2 the steering angle error (θ_e) and lateral distance error (d) of the AGV can be obtained by the information provided from the Hall-effect sensor passing the magnet spots.

After finding the error against the reference guidance line of the AGV, the steering angle of the AGV should be determined to reduce this error. This implies obtaining the position changes

Sensor	Step	FnL	Ref (Reference Path)	Fnc (Actual Path)	FnR
F1	t	81	530	532	80
F2	t+1	75	530	534	82
F3	t+2	81	530	538	80
F4	t+3	76	530	531	81
F5	t+4	80	530	530	80
F6	t+5	78	530	532	82
F7	t+6	82	530	536	80
F8	t+7	81	530	532	82
F9	t+8	79	530	534	81
F10	t+9	80	530	533	80
F11	t+10	81	530	528	85
F12	t+11	82	530	530	86
F13	t+12	79	530	536	82
F14	t+13	76	530	534	81

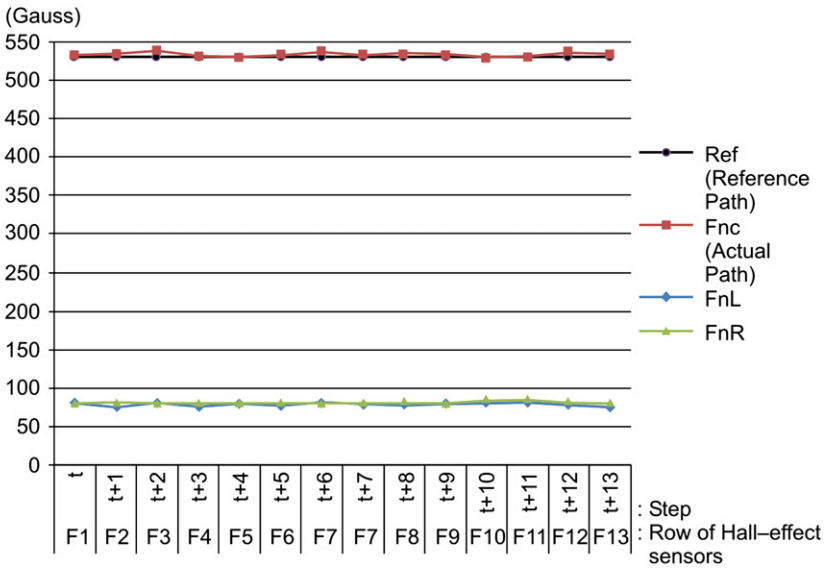

Fig. 5-2. Distribution of magnetic flux density (Gauss) measured by the Hall-effect sensor when passing magnet spots during straight forward navigation.

Sensor	Step	FnL	Ref (Reference Path)	Fnc (Actual Path)	FnR
F1	t	81	530	532	80
F2	t+1	80	530	533	80
F3	t+2	81	530	532	80
F4	t+3	80	530	533	80
F5	t+4	73	530	491	135
F6	t+5	76	530	503	108
F7	t+6	81	530	528	80
F8	t+7	81	530	532	79
F9	t+8	79	530	534	81
F10	t+9	80	530	533	80
F11	t+10	80	530	532	80
F12	t+11	81	530	532	80
F13	t+12	79	530	534	81
F14	t+13	80	530	534	81

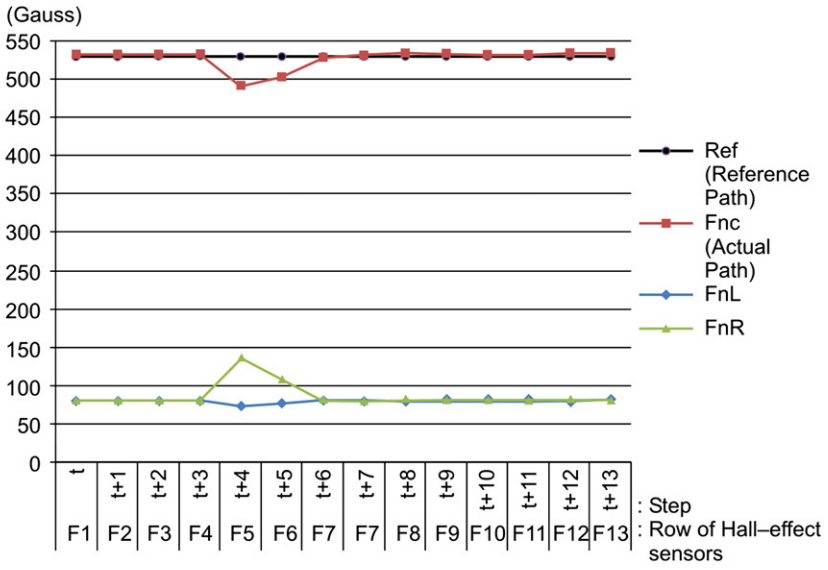

Fig. 5-3. Distribution of magnetic flux density (Gauss) measured by the Hall-effect sensor when passing magnet spots during straight forward navigation with disturbances on step $(t+3)$ and step $(t+4)$.

$(\Delta x,\ \Delta y,\ \Delta\theta)$ during the next scanning step, ΔT, and the speed of the left and right wheels to accomplish this position changes based on the lateral path plan.

The steering angle is then determined. Using the angular velocities (w_L, w_R) of both the left and right wheels provided by the encoder, the position change $\Delta x = \Delta s\cos(\theta+(\Delta\theta/2))$, $\Delta y = \Delta s\sin(\theta+(\Delta\theta/2))$, $\Delta\theta = ((\Delta s_R - \Delta s_L)/D)$ is computed using the equation of motion of the AGV. In additional, the distance movement is compared with the reference values for the AGV navigation using the proximity sensor for the counter attached to the driving wheel of the AGV.

5.3. Straight navigation method when switching from dead reckoning (undetected magnet spot) to magnet spot environment

The dead reckoning navigation method is used when the magnet spot is not detected during the AGV navigation. The encoder and counter are used to check the position movement. If the AGV is moved to the next magnet spot uneventfully avoiding any large position error, the Hall-effect sensor will provide meaningful navigation information again.

This implies that θ_e and d can be obtained at the instant when the Hall-effect sensor scans the next magnet spot. Using this error information, θ_e and d can be corrected again.

5.4. Straight navigation method with the occurrence of lateral distance error (d) and steering Angle error (θ_e)

Figs. 5-4 and 5-5 illustrate the results of the experiment with the method proposed in this study and path-tracking simulation when d and θ_e occurred while the AGV was moving straight forward. They show that the AGV tracks the desired target path of F_{nC} line successfully.

Sensor	Step	FnL	Ref (Reference Path)	Fnc (Actual Path)	FnR
F1	t	79	530	23	2
F2	t+1	550	530	70	26
F3	t+2	81	530	550	82
F4	t+3	26	530	75	520
F5	t+4	59	530	448	86
F6	t+5	78	530	479	40
F7	t+6	92	530	516	65
F8	t+7	81	530	538	82
F9	t+8	79	530	550	81
F10	t+9	80	530	533	80
F11	t+10	81	530	548	85
F12	t+11	82	530	530	86
F13	t+12	79	530	536	82
F14	t+13	76	530	534	81

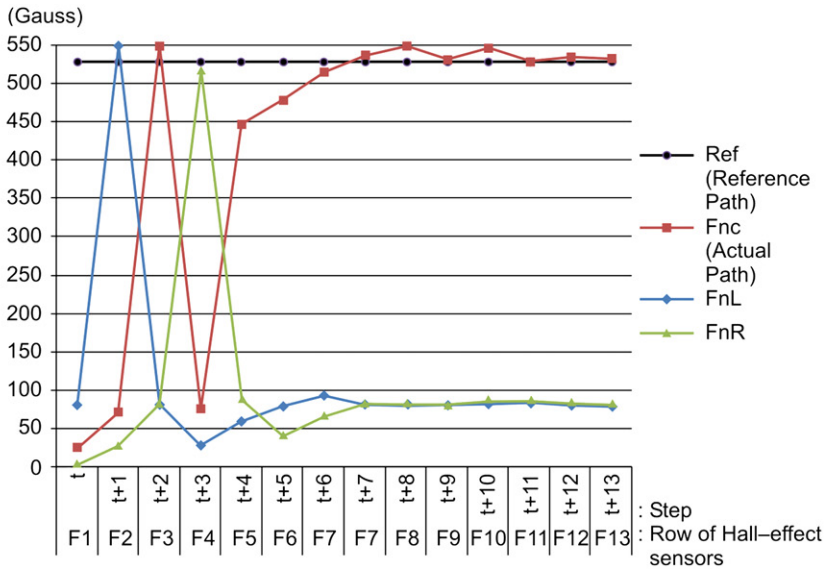

Fig. 5-4. Path tracking result for AGV moving at a linear velocity of $v=1$ m/sec with a lateral distance error of $d=90$ mm and steering angle error of θ_e.

Sensor	Step	FnL	Ref (Reference Path)	Fnc (Actual Path)	FnR
F1	t	509	530	75	20
F2	t+1	75	530	470	166
F3	t+2	108	530	506	72
F4	t+3	76	530	531	91
F5	t+4	80	530	550	80
F6	t+5	78	530	532	82
F7	t+6	82	530	536	80
F8	t+7	81	530	532	82
F9	t+8	79	530	534	81
F10	t+9	80	530	533	80
F11	t+10	81	530	528	85
F12	t+11	82	530	530	86
F13	t+12	79	530	536	82
F14	t+13	76	530	534	81

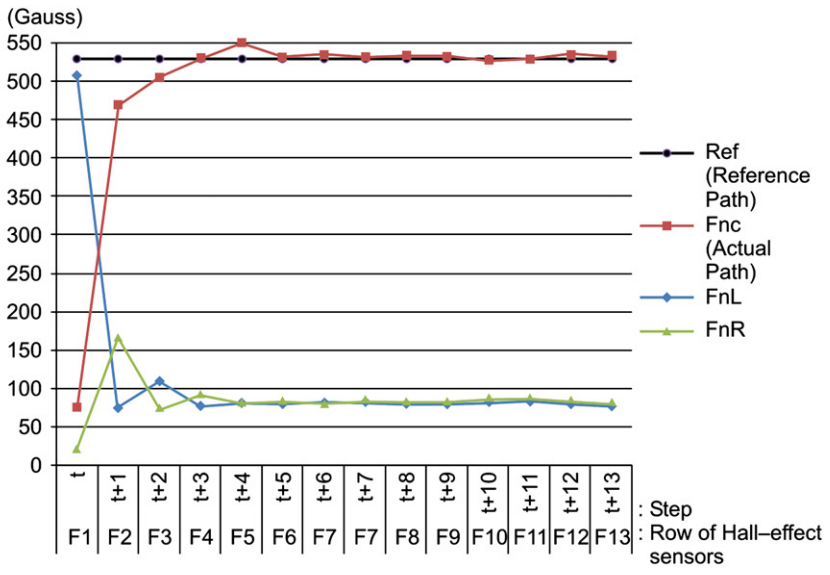

Fig. 5-5. Path tracking result for AGV moving at a linear velocity of $v=1$ m/sec with a lateral distance error of $d=30$ mm and steering angle error of θ_e.

6. Conclusions

In this study, a magnet guidance method for the indoor navigation of AGV has been proposed; cylindrical magnet spots were used for the navigation guide. High-speed high-precision navigation were the aims of this AGV navigation method, and Hall-effect sensors, encoder, and counter were used for continuous guidance even when no magnet spot was detected.

This method resulted in continuous guidance and achieved stable and satisfactory navigation with high speed and precision. In addition, other guidance methods are generally difficult to install, require high costs, large spaces, and heights for installation, and difficult to maintain/repair; as a result, their control algorithms are very complex. However, our method used magnet spot guidance and Hall-effect sensor to overcome these advantages.

External errors occur due to skidding (slipping) of the wheel and uneven floor surface while tracking the guidance path. These errors are impossible to measure with only an encoder and require external sensors such as gyro sensors. However, in this study, an encoder and counter were installed at the driving wheel of the AGV for error measurement and correction by the dead reckoning method. The distribution of the magnetic flux density radiating from magnet spots was measured with Hall-effect sensors; the Hall-effect sensor measures the distribution of the magnetic flux density of the next magnet spot to calculate the steering angle for reverting to the guidance path. A fuzzy algorithm was used to correct for the error due to skidding (slipping) of the AGV wheel on a real-time basis in order to navigate straight or rotate.

The proposed method was found to be robust to disturbances and uncertainty problems of tracking the reference paths through experiment. Furthermore, its position control capability, effectiveness of accurate navigation control, and system stability were verified in real production processes.

References

[1] Vis IFA. Survey of research in the design and control of automated guided vehicle systems. European Journal of Operational Research 2006;170:677–709.
[2] Kamewaka S, Uemura S. A magnetic guidance method for automated guided vehicle. IEEE Transactions on Magnetics 1987;23(5):2416–8.

[3] Freund E, Dierks F. Laser scanner based free navigation of autonomous vehicle. Control Engineering Practice 1994;2(2):299–304.
[4] Wu S-F, Mei J-S, Niu P-Y. Path guidance and control of a guided Wheeled mobile robot. Control Engineering Practice 2001;9:97–105.
[5] Cole SB. Magnetic field-based navigation of a mobile robot. Ann Arbor, Michigan: ProQuest Co; 2005.
[6] E. Ramsden, Hall-effect sensors: theory and application, Elsevier-Newnes, Oxford, 1998.
[7] Brauml T. Embedded robotics: mobile robot design and applications with embedded systems. 2nd ed. Berlin Heidelberg: Springer; 2006. p. 98–9.
[8] Siegwart R, Nourbakhsh I. Introduction to autonomous mobile robots. MIT Press; 2004. p. 186.
[9] SICK sensor intelligence, NAV200 Laser positioning system for navigational support; 2006. p. 77. 8011502/R197/2007-02-12.
[10] Masutani Y, Mikawa M, Maru N, Miyazaki R. Visual servoing for nonholonomic mobile robot. In: Proceedings of IEEE international conference on intelligent robots and systems, vol. 2; 1994. p. 1133–40.
[11] Fukao T, Nakagawa H, Adachi N. Adaptive tracking control of a nonholonomic mobile robot. IEEE Transactions on Robotics and Automation 2000;16(5):609–15.